Electronic structures of zigzag graphene nanoribbons with edge hydrogenation and oxidation

Geunsik Lee and Kyeongjae Cho*
Department of Materials Science and Engineering and Department of Physics, The University of Texas at Dallas, Richardson, Texas 75080, USA

(Received 8 September 2008; published 29 April 2009)

Using the *ab initio* density-functional theory method and local spin-density approximation, we calculated the electronic band structures of H or H2 edge-hydrogenated zigzag graphene nanoribbons (ZGNRs) as well as COH, CO, or C2O edge-oxidized ZGNRs. We found that the OH group yields almost the same band structure as the sp^2 hybridization of H edge, and that the ketone (CO) and ether (C2O) groups result in band structures similar to those of sp^3 hybridization of H2 edge. Compared to H passivation, edge oxidation by the ketone or the ether group is energetically more favorable, suggesting that the GNR's edges will be oxidized in the presence of oxidizing species. Edge oxidized GNRs show metallic band structures caused by the larger electronegativity of oxygen relative to carbon, and these findings raise a question about the physical origins of the experimental observations of semiconducting GNRs. Such discrepancy suggests that more realistic modeling of GNR edge structures will be necessary to understand the experimental findings.

DOI: 10.1103/PhysRevB.79.165440 PACS number(s): 73.22.−f, 72.80.Rj, 73.20.At, 75.70.Ak

I. INTRODUCTION

Graphene is a single atomic layer of graphite and has attracted intensive research interests because of technologically promising electronic properties.[1] Its electronic structure near the Fermi level is determined by the π-orbital band structure and has a zero gap at the Dirac point with linear energy-momentum dispersion. The corresponding carrier motion is governed by the Dirac-type Hamiltonian (rather than by the Schrödinger equation) with the Fermi velocity as high as 10^6 m/s. The measured mobility was very high (up to 15 000 $cm^2/V\,s$) owing to ballistic transport on a submircrometre scale at 300 K.[2–4] Graphene has been studied seriously for future nanoelectronic device applications such as field-effect transistors (FETs) and chemical sensors.[5–10] However, a pristine graphene sheet does not have a finite-energy gap and always shows a minimum conductivity caused by impurities or substrate effects.[11,12] In order to fabricate FETs with desirable on-off ratios, a band gap must be opened, and one such route is the formation of graphene nanoribbons (GNRs).[13,14]

All GNRs have been measured to have *transport energy gaps* which are inversely proportional to the ribbon width W.[13,14] The energy gap of lithographically formed GNRs was fitted by $E_g=\alpha/(W-W^*)$ with $\alpha=0.2$ eV nm and $W^*=16$ nm.[13] In this measurement, a GNR of width W was shown to have an electronically inactive edge of width W^* so that the electronically active part of the ribbon has the width of W-W^*. The inactive part may involve a rough edge shape and saturated C-π orbitals by O atoms, both of which are introduced by oxygen plasma etching. In another recent experimental study of chemically formed GNRs, the energy gap showed the dependence of E_g (eV)$=0.8/W$ (nm).[14] Unlike lithographically formed GNRs, such GNRs have ultrasmooth edge structures, but the measured mobility is quite low
($\sim$200 $cm^2/V\,s$) which is most likely due to adsorption of many molecules and other chemical impurities during the synthesis.[8]

Theoretical electronic structures of diverse GNRs have been extensively investigated using the tight-binding (TB) method and the *ab initio* density-functional theory (DFT) method. Early TB studies in 1996 have shown that ideal GNRs with zigzag edges (ZGNRs) are metallic and are independent of the ribbon width and that ideal GNRs with armchair edges (AGNRs) have band gaps corresponding to the ribbon width.[15] A subsequent *ab initio* calculation confirmed the metallic band structure of ZGNR using the local-density approximation (LDA).[16] Such dependence of GNR's metallic behavior on the chirality is not consistent with experimental results.[13,14] However, recent *ab initio* calculations have shown that both ideal ZGNRs and AGNRs have band gaps induced by edge magnetization (for ZGNR) and edge structure relaxation (for AGNR).[17] The experimentally measured gaps seem to agree with the calculated band gaps of ideal GNRs.[17,18] However, there are two important factors to be examined before concluding that the experimental energy gaps are explained by the band gaps of ideal GNRs. First, it is well known that the LDA method significantly underestimates the band gaps, and that the GW band structures provide more accurate band gaps which are significantly larger than LDA band gaps. Therefore, the apparent agreement between the LDA band-gap values and the experimentally measured band gaps does not prove that the theoretically predicted ideal GNR band gaps are experimentally validated. Recent GW calculation has revealed a significant amount of band gap increase (larger than 1 eV) for both types of GNRs.[19] Furthermore, the GNR structures used in theoretical studies have straight edge structures with C-H edge passivation of edge carbon atoms. This ideal structure is very far from realistic edge structures of experimentally used GNRs. Realistic modeling must incorporate irregular edge shape, variation of edge chemistry, and effect of charged impurities as evidenced by experimental and theoretical studies.[11,12,20–24]

The effect of edge roughness on the GNR band gap was studied by quantum transport simulations.[20–22] It has been shown that while the presence of irregular edge shapes dramatically decreases conductance near zero voltage for metal-

lic AGNRs, it has no such significant effect for ZGNRs. This implies that the edge roughness alone is not the dominant cause of the measured GNR energy gaps (note that experiments have shown that all GNRs are semiconductors independent of chirality). The effect of edge chemistry has been studied for ZGNRs with one edge termination modified from C-H (sp^2 σ-bonded edge C) to C-H2 (sp^3 σ-bonded).[23,24] These calculations showed that the edge-modified GNRs have ferromagnetic edge magnetization and that the edge magnetic moments can be coupled ferromagnetically or antiferromagnetically with net magnetic moments, where zero-gap band structures were reported. The main focus of these papers is the magnetic moments of GNRs rather than the edge modification effects on the band gaps, and the edge passivation by H or H2 is not comprehensive enough to cover the realistic edge chemistry. The effect of charged impurities has been studied recently, using the Boltzmann transport equation.[12] However, we have not seen similar studies that consider microscopic model and quantum mechanics which are necessary to take into account phase interference effect in such nanometer scale systems.

Although both edge roughness and edge chemistry effects should be considered for more realistic modeling of GNRs, this paper focuses on the variation of edge chemistry through hydrogenation as well as oxidation of the ribbon edges. The results of this study will provide the necessary understanding on the edge chemistry effects on the electronic structures of ideal GNRs and facilitate the study including both effects later on. From the GNR fabrication procedure via oxygen plasma etching[13] or intercalation of oxidizing acids,[14] oxidation would be the most abundant reaction occurred at the edges. Recently, the stability and energy gap of edge-oxidized ZGNRs have been calculated using the *ab initio* method based on the Gaussian package.[25] In that study, a ZGNR with 8 zigzag chains (8-ZGNR) was used with different chemical edge terminations including the hydroxyl (C-OH), lactone, ketone, and ether groups. The calculated band gaps are large (0.77–1.05 eV) for most edge terminations (including C-H passivation), with the exception of ketone group (CO) termination, which yields a 0.03 eV band gap. Specifically, the band gap of the 8-ZGNR with ideal C-H termination is 1 eV, which is significantly larger than the LDA band gap of 0.3 eV. Another paper has studied the ZGNR band gap with edge functionalizations by NH_2, OH, COOH, NO_2, and O.[26] It was shown that most of them show a semiconductorlike band gap, but O functionalization in the form of the ketone group shows the metallic density of states (DOS), which is consistent with the small gap of the previous report.[25] Since materials are usually transformed into insulators upon oxidation, the above two theoretical reports have shown the seemingly unexpected result that certain oxidized GNRs have a semimetallic gap. The recent theoretical study on edge functionalized graphene finite cluster has shown that the p electrons of an oxygen atom participate in the π-electron system to cause gap states.[27] However, the DOS alone is not enough to determine the metallic or semiconducting character of the system, because localized states may appear near the Fermi level resulting in a zero gap as shown in Anderson insulators.[28] Therefore, it is important to calculate band structures of edge-oxidized GNRs to understand the transport property from their dispersions. Even though the band gaps of edge-oxidized GNRs are reported, the band structures and the origins of the electronic structures near the Fermi level have not been investigated in details yet.

In this paper, we investigated the ZGNR band structures with edge-chemistry modifications by H and O atoms, using the *ab initio* DFT method within LDA and local spin-density approximation (LSDA). In Sec. II, details of the calculation are given. Our calculated results are presented in Sec. III, where we start with bare ribbons, and then consider the homogeneous chemical structure along each edge, and either same or different chemical modifications at two edges. In particular, we show how edge oxidation, compared with H passivation, affects the ZGNR band structure, revealing the metallic band structure for edge-oxidized ZGNR. In Sec. IV, we primarily discuss the origin of ZGNR metallic band structure. A summary is given in Sec. V.

II. METHOD

For calculation of the *ab initio* electronic band structures of ZGNRs, we used the Vienna *ab initio* simulation package (Ref. 29) with its projected augmented wave pseudopotentials[30] within the LSDA scheme.[31] Although the LSDA method is not reliable in accurate prediction of the energy gap, the comparison of the energy gaps for the graphene nanodot system by GGA and B3LYP functionals has shown that the qualitative trend does not change.[27] Also for extended electronic structure calculations, rather than finite cluster as adopted in Ref. 27, LDA and LSDA are well-established methods. We used an energy cutoff of 400 eV for the plane-wave basis in the program. We included a vacuum region of 10 Å to minimize the interaction between periodic images of the ribbon. A Monkhorst-Pack k grid of $15\times1\times1$ is used for the one-dimensional (1D) Brillouin zone (BZ). The geometries of ZGNRs studied here are relaxed until the force is less than 0.01 eV/Å. Our calculation scheme yields a total-energy error of $\delta E\sim1$ meV/atom. For the DOS calculations, we used the tetrahedron integration method with a $23\times1\times1$ k grid followed by broadening with the Gaussian width of 0.25 eV.

All of the ZGNRs studied here have the width of eight zigzag chains ($N_Z=8$, $W=1.6$ nm), unless specifically mentioned. We have chosen $N_Z=8$ because it is commonly used for ZGNR electronic structure studies,[17,19,25] but the conclusions of our study are valid for ZGNRs with different N_Z for both even and odd numbers of zigzag chains. The unit cell consists of 16 C atoms for the bare part with additional H or O atoms attached to chemically modify the edges. We consider five kinds of chemical edge modification: single hydrogen (CH), double hydrogen (CH2), hydroxyl (COH), ketone (CO), and ether (C2O). Their structures are shown in Fig. 1, where there are two possible geometries for the hydroxyl group, COH-α and COH-β. We denote the edge and the inner edge C atoms by C1 and C2, respectively. To modify two edges of a ZGNR, we combine two of the edge structures shown in Fig. 1, and represent the resulting ZGNR as A-B (A,B=CH, CH2, COH, CO, and C2O) throughout this paper.

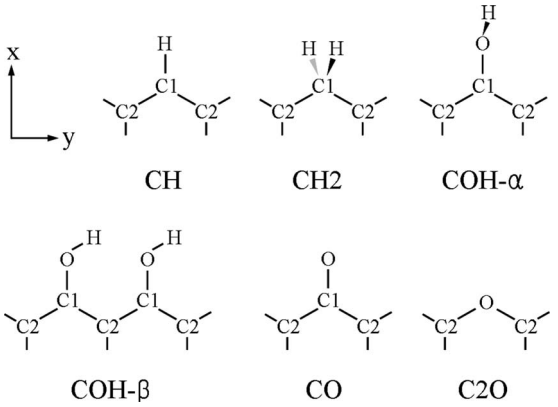

FIG. 1. Chemical modifications of a zigzag graphene nanoribbon (ZGNR) edge. CH: a single hydrogen, CH2: two hydrogens, COH: a hydroxyl group, CO: a ketone group, C2O: an ether group. The C1 and C2 means carbon atoms located at the edge and the inner edge sites, respectively. The H atoms, except for CH2 and COH-α, are on the graphene plane. In the COH, there are two possible configurations which are denoted by COH-α and COH-β. At the top-left corner, the coordinate axis is provided for the atomic-orbital analysis later.

We also performed three kinds of spin-polarized calculation for all of the ZGNRs: nonspin polarization (PM), ferromagnetic ordering along each edge and antiparallel spin orientation between the two edges (FA), and ferromagnetic spin coupling for all electrons (FF). The relaxed atomic structure with the PM configuration is used to calculate the band structure, and also spin densities and their band structures for the other two kinds of spin configuration. To estimate the errors, we have checked the effect of spin polarization during atomic relaxation for the OH functionalized ribbon, and the total energy and the atomic position change less than 0.5 meV per unit cell and 0.005 Å, respectively, compared to those of static calculation for a given spin configuration.

III. RESULTS

We first show the band structure of bare ZGNR and study the effect of chemical edge modification and its stability by calculating binding energies for hydrogenation or oxidation to form each of six edge structures shown in Fig. 1. Then we present band structures of ZGNR with either hydrogenation or oxidation at both edges and combination of both types.

A. Band structure of bare ZGNR and binding energies for edge modifications

In Fig. 2, we show the band structure of bare ZGNR for three types of spin configurations which are PM, FA, and FF. In the bare ZGNR, shown in Fig. 2(a), most carbon atoms have three nearest neighbors like pure graphene, but the edge carbon atom (C1) has only two neighbors. It means that the C1 has one orbital not participating in its sp^2-σ bonding. Since there are two C1 atoms from both edges in the unit cell, two such orbitals will give two flat bands without taking into account spins. From Fig. 2(b), we see two degenerate bands crossing the Fermi level. Although the two degenerate

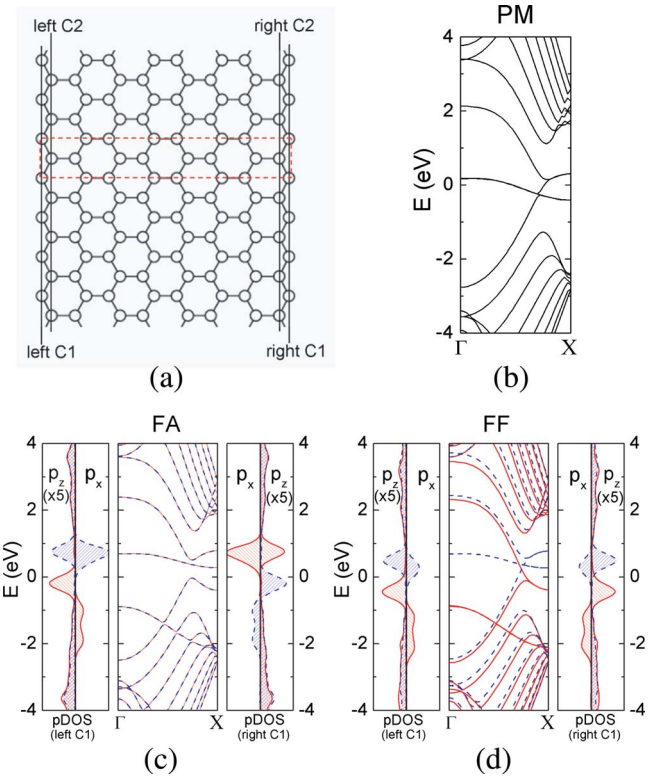

FIG. 2. (Color online) (a) Top view of bare ZGNR. The edge and inner edge carbon atoms are indicated by C1 and C2 for the left and right edges. The unit cell, indicated by the red dashed line, consists of 16 carbon atoms. Its band structures are shown for (a) PM (without spin polarization), (b) FA (ferromagnetic spin ordering at each edge and antiparallel spin orientation between both the edges), and (c) FF (ferromagnetic spin orderings at each edge and between both the edges) spin configurations. For the FF and FA, spin-up and down states are represented by the red solid and blue dashed lines in the band structure and projected density of states (pDOS). The pDOS is shown for two dangling-bond orbitals (p_x and p_z) of the C1 atoms at the left and right edges, where p_z pDOS is magnified five times.

bands are expected to be half filled by two electrons from the dangling σ bonds, it is more than half filled as seen from Fig. 2(b). Additional population comes from the C1's π electron. From the 16 π electrons in the unit cell, there are eight occupied π bands and eight unoccupied π^* bands. Due to the presence of dangling π bonds at C1, the highest π (π-top) and the lowest π^* (π^*-bottom) bands are flat and degenerate near the X point. While those flat bands are half filled at the Fermi level in case of CH-CH passivated ZGNR,[15] they are empty in case of Fig. 2(b) to donate the π electrons to the dangling σ bonds.

By imposing spin polarization in forms of FA and FF, we see the splitting of the degenerate flat σ and π bands, which are shown in Figs. 2(c) and 2(d). We represented spin-up and down bands by the red solid and blue dashed lines, respectively, in the band structures. For the FA, shown in Fig. 2(c), the flat bands (caused by the dangling σ and π bonds) show substantial amount of splitting while keeping spin-up and down degeneracy. The bands by the dangling σ bonds are significantly lowered for the filled states and a little above

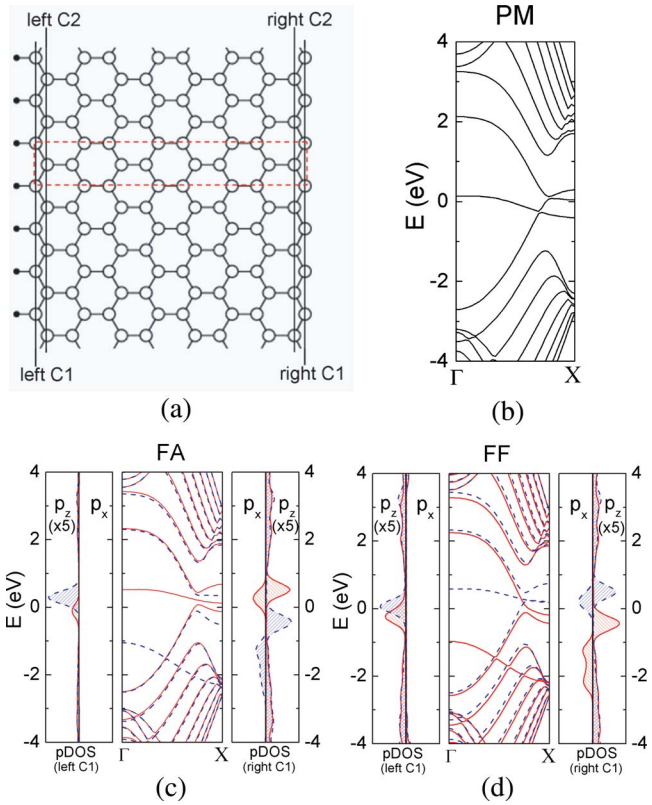

FIG. 3. (Color online) (a) Top view of ZGNR with the left C1 atom passivated by a single H atom, and its band structures for (a) PM, (b) FA, and (c) FF spin configurations. The meanings of color scheme and legends shown in this figure are the same as those of Fig. 2.

the Fermi level for the empty ones. Also the flat π-top and π^*-bottom bands shift below and above the Fermi level. Such splitting causes an indirect energy gap opening of 0.3 eV. The split spin-up and down bands are localized at the edges in a symmetrical manner. It can be seen in the projected density of states (pDOS)[32] which is shown in the left and right-hand sides of the band structure for the left and right C1 atoms, respectively. The p_x and p_z of C1 correspond to the orbitals of dangling σ and π bonds. For the filled bands of dangling σ bonds (p_x orbitals), spin-up (red solid line) and down (blue dashed line) states are localized at the left and right C1 atoms, and vice versa for the empty bands. The bands by dangling π bonds (p_z orbitals) show the same trend. This results in a net spin magnetic moment of zero. For the FF, shown in Fig. 2(d), the spin-up (down) bands are filled (empty) in both flat σ and π bands with the degeneracy of two. The two degenerate bands are related with the left and right dangling bonds as can be seen from the pDOS. This results in a net magnetic moment as large as $2.5\mu_B$. The ferromagnetic ordering of the flat π band gives a zero energy gap. The total energies for the FA and FF are lower than that of PM by 0.41 and 0.40 eV per unit cell.

We investigate the effect of edge chemistry modification by passivating the σ orbital of the left C1 with a single hydrogen, which is shown in Fig. 3. Since the passivated σ orbital is stabilized, the corresponding state (p_x in pDOS at the left) does not appear in the range $-4 \leq E \leq 4$ eV. Thus, the degeneracy of the flat σ band is one in case of PM [Fig. 3(b)], not two like the bare ZGNR. Most of the features that we have seen in the bare ZGNR are retained including spin-polarization effects. The minor difference is that the flat π-top and π^*-bottom bands are not degenerate already in the case of PM, because the mirror symmetry of both edges is broken. The total energies of the FA and FF are 0.21 eV/u.c. lower than that of PM in this case, which is half of the energy in the bare ZGNR.

TABLE I. The binding energy (E_b) for a particular type of edge modification, i=CH, CH2, COH-α, COH-β, CO, and C2O is shown in Fig. 1. The unit of E_b is eV per atom (O, H) for i=CH, CH2, CO, C2O, or hydroxyl group (OH) for i=COH-α and COH-β.

Type of edge structure	E_b
CH	5.73
CH2	4.05
COH-α	8.05
COH-β	8.93
CO	8.00
C2O	9.09

The stability of different chemical structures at the edge is studied by calculating the binding energy (E_b) for a particular type of edge modification, which is listed in Table I. We vary the edge chemistry type as i=CH, CH2, COH-α, COH-β, CO, and C2O as shown in Fig. 1. The reference system for obtaining E_b consists of the bare ZGNR plus isolated H or O atoms for i=CH, CH2, CO, C2O, and OH groups for i=COH-α and COH-β. The unit of E_b is eV per atom (O, H) or hydroxyl group (OH). One can see that the binding energy for oxidation is much larger than that for hydrogenation. This indicates that the oxidation is much more favored than hydrogenation for a given bare ribbon. The largest binding energy is obtained for the C2O type, where one can see two C-O bonds after oxidation from Fig. 1. Although the formation energy of the whole ribbon with C2O edges is almost zero from Ref. 25, the ZGNR without C1 atoms at the edges (see C2O in Fig. 1) is highly reactive to be oxidized from our calculation. The E_b for COH-α and CO is very similar, because they involve a single C-O bonding. However, COH-β results in a rather large binding energy because of hydrogen bonds along the longitudinal direction.

B. Edge hydrogenation

We have calculated the band structures of ZGNR with the edge chemistry modified in three forms which are single hydrogen passivations (CH-CH) and double hydrogen passivations (CH2-CH2) at both edges, and their combination (CH2-CH). Our results show that the H or H2 edge modification causes sp^2 or sp^3 hybridization of edge C1 atoms resulting in dangling π bonds at the edge C1 or C2 atoms, respectively. Their flat π-top and π^*-bottom bands concerned with the dangling π bonds appear in different range of wave vector k. The band gap opening by spin polarization is confirmed, but

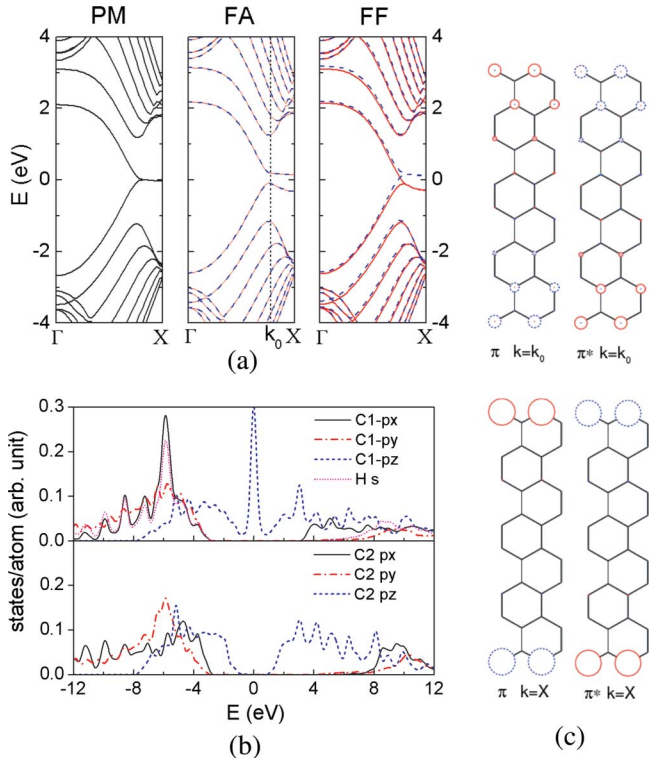

FIG. 4. (Color online) CH-CH: the CH type at both edges. (a) The band structures for three kinds of spin configuration. PM: without spin polarization, FA: ferromagnetic spin ordering at each edge and antiparallel spin orientation between both the edges, FF: ferromagnetic spin ordering between both the edges. Spin-up and down bands are drawn by red solid and dashed blue lines, respectively. (b) The projected density of states for C1 and C2 atoms for the PM. The C1 and C2 atoms mean the edge and the inner edge carbon atoms as given in Fig. 1. (c) The spatial map of carbon π-orbital contributions for specific states in the FA band structure of (a). The π and π^* mean the valence-top and the conduction-bottom bands, respectively, and the position k_0 is indicated by the vertical dotted line in (a). The red solid and blue dashed circles mean spin-up and down states, and the circle size is proportional to the contribution.

the relative stability of the spin induced gap is very small (2 meV/u.c.).

1. CH-CH

Figure 4 shows the calculated electronic structures of the CH-CH ZGNR for which each edge C atom is passivated by a single H atom for sp^2 hybridization. In Fig. 4(a), the band structures are shown for PM, FA, and FF spin configurations. The unit cell consists of 16 C and two H atoms, which yield 16 π electrons. From the 16 π electrons, there are eight occupied π bands, and eight unoccupied π^* bands. Below (above) the π (π^*) bands, there are σ (σ^*) bands formed by C-sp^2 orbitals.

In the PM band structure of Fig. 4(a), the highest π (π-top) and the lowest π^* (π^*-bottom) bands are flat and degenerate near the X point, as reported by tight-binding[15,24] and LDA (Ref. 16) calculations. This zero gap arises from the Dirac point of graphene which folds into $k=2\pi/3$ of the ZGNR BZ. These π-top and π^*-bottom bands are flat for $2\pi/3 \leq k \leq \pi$ keeping the zero gap to satisfy the convergence condition, $|1+e^{ik}|=|2\cos(k/2)| \leq 1$.[15] If we take into account spin polarization based on the LSDA scheme, the total energy is likely to be lowered through degeneracy breaking. In the FA band structure in Fig. 4(a), one can see that the π-top and the π^*-bottom bands move down and up, respectively, keeping the degeneracy between both spins. Such a band gap opening was first reported by Son *et al.*[17] On the other hand, for the FF of Fig. 4(b), there is no such gap opening, because either one of spin-up or down band tends to be occupied to cause the system to become ferromagnetic. As a result, each spin band cross the Fermi level near $k=2\pi/3$. From those changes of electronic eigenvalues, the FA configuration has the lowest total energy ($E_{FA}=-29$, $E_{FF}=-27$ meV/u.c. relative to E_{PM}). The spin magnetic moment is zero for FA, but $0.46\mu_B$ per unit cell for FF.

It is well known that the states in the flat band region represent edge states which are strongly localized at the edge C atoms.[15–17,24] In the pDOS in Fig. 4(b), the π orbital of the edge carbon atom (C1-p_z) shows a large peak at the Fermi level, whereas the inner edge carbon atom (C2-p_z) does not contribute at all. This indicates that the edge states are highly confined at the edges. All the other π or π^* states, in the range of $-8<E<0$ eV or $0<E<12$ eV, consist of π orbitals of all the C atoms. Below -4 eV, there are σ bands formed by C-p_{xy} orbitals. By imposing the FA spin coupling, the spin-up and down edge states are split into opposite edges, as shown in Fig. 2(c). For the edge states of Fig. 4(c), we have chosen the π-top and the π^*-bottom bands at $k_0=0.78\pi$ [indicated by the vertical dotted line in the Fig. 2(b)-FA] and $k=X$. From Fig. 4(c), each spin state switches its localization side between the π-top and π^*-bottom bands. Also, the C atom closer to the edges has the larger π-orbital contribution, and $k=X$ states are highly confined at the edges.

From Fig. 4(c), we see that different spin states have π-orbital contributions from different sublattices of the honeycomb lattice. For $k=k_0$, which corresponds to the smallest direct gap, residual amplitudes of spin-up and down states cause a very small amount of antiferromagnetic interaction near the center of the ribbon, giving rise to the energy gap opening. We predict that the wider ribbon has a smaller interaction near the center, so the resulting energy gap would be inversely proportional to the width.[13,17] However, the direct gap at $k=X$ will not be sensitive to the ribbon width, because the spin-spin interaction between highly confined states at the opposite edges is negligible.

2. CH2-CH2

Figure 5 shows the electronic structures of the CH2-CH2 ZGNR. Its band structure for the FA spin configuration is shown in Fig. 5(a), which gives the same dispersion as those of PM and FF configurations. Since there is no electronic energy level shift by the different spin configurations, the calculated total energies for the three spin configurations are nearly the same, and their spin magnetic moments are zero.

One of the TB studies has shown that there are degenerate flat bands with the zero gap and that the criteria for their states to have regular wave functions is $|1/(1+e^{ik})| = |1/2\ \cos(k/2)| \leq 1$, that is $0 \leq k \leq 2\pi/3$.[24] Our *ab initio* re-

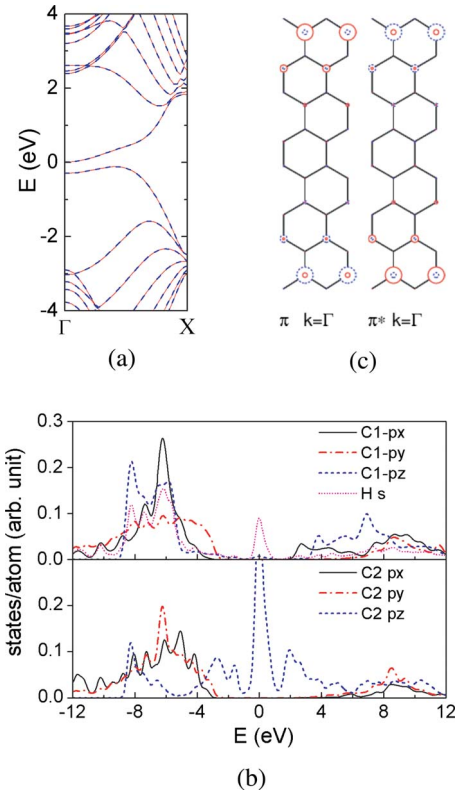

FIG. 5. (Color online) CH2-CH2: the CH2 type at both edges. (a) The band structure for the FA configuration. The others for PM and FF have the same dispersion as shown above. (b) The projected density of states for C1 and C2 atoms for the PM. (c) The spatial map of carbon π-orbital contributions for the valence-top (π) and the conduction-bottom (π^*) bands at $k=\Gamma$ in (a). The red solid and blue dashed lines represent spin up and down states, respectively, in (a) and (c).

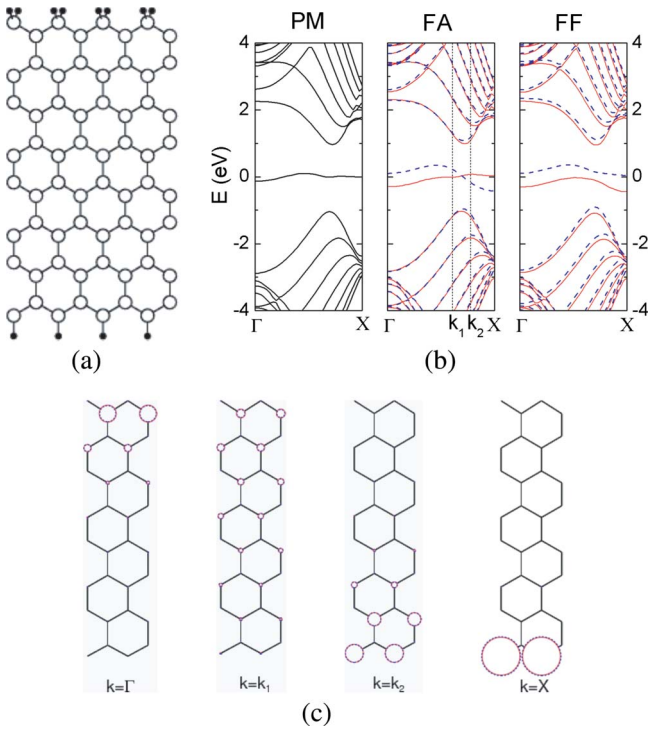

FIG. 6. (Color online) CH-CH2: the CH or CH2 type at each edge. (a) Top view of a ZGNR with the CH-CH2 type. (b) The band structures for PM, FA, and FF spin configurations. Red solid and blue dashed lines represent spin-up and down bands, respectively. (c) The spatial map of carbon π-orbital contributions for the flat spin up and down bands near the Fermi level in the FA of (a). The $k=\Gamma$, $k_1(=11\pi/18)$ and $k_2(=7\pi/9)$, are chosen, where k_1 and k_2 are indicated by the vertical dotted lines in (a). The spin-up and down states have the same magnitude in their contributions, overlapping each other at all C sites.

sult in Fig. 5(a), however shows a nonzero energy gap with a slight dispersion within that k range. This nonzero energy gap is different from the gap caused by antiferromagnetic interaction in the CH-CH case [FA in Fig. 4(a)]. The dispersive characteristic makes the indirect gap zero, but the direct gap at $k=\Gamma$ is 0.28 eV.

From the pDOS of Fig. 5(b), one can see that the π-top and π^*-bottom states for $0 \leq k \leq 2\pi/3$ (which we still call edge states) are highly localized at the inner edge C atoms (C2-p_z), although there is a small peak from the H-s orbital at the Fermi level. The C1-p_z appears at a low-energy level to form σ bonds with two H-s orbitals together with the C1-p_x orbital, giving sp^3 hybridization of the C1 atom. The spatial maps of π-orbital contributions for the edge states are shown in Fig. 5(c), and they are very similar to those of Fig. 4(c). However, there are nonvanishing contributions from the bulk C atoms, which are related to the slight dispersion of the edge states.

3. CH2-CH

Figure 6(a) shows a top view of the CH2-CH ZGNR. Its band structures for three spin configurations are shown in Fig. 6(b). The PM band structure in Fig. 6(b) has an almost flat band at the Fermi level, as predicted by TB calculations.[24] For FA and FF cases, however, the dispersion of the flat band is more pronounced. While the band structures are metallic for PM and FA, the spin-up (down) band for FF is fully occupied (unoccupied) with a direct energy gap of 0.41 eV at Γ (the indirect gap is nearly zero). Since each spin band is partially occupied for FA and fully occupied or unoccupied for FF, the total energy is lowest for FF ($E_{\mathrm{FF}}=-39$, $E_{\mathrm{FA}}=-28$ meV/u.c. relative to PM). The spin magnetic moments were calculated to be 1.0 for FF and $0.4\mu_B$ for FA. Our LSDA band structure for FF is consistent with that reported by Kusakabe *et al.*[23]

Figure 6(c) shows the spatial π-orbital contribution map of the flat spin-up and down bands near the Fermi level for the FA case. We choose $k=\Gamma$, $11\pi/18$ (indicated by k_1) wave vectors for $0 \leq k \leq 2\pi/3$ and $k=7\pi/9$ (indicated by k_2), and X wave vectors for the range $2\pi/3 \leq k \leq \pi$. We can see that the former states are localized into the CH2 part and the latter into the CH. The edge states for $k=\Gamma$, k_1 are localized at the inner edge atoms (C2) of the CH2 part, and those for $k=k_2$, X are at the edge atoms (C1) of the CH part. This characteristic does not change for the PM and FF spin configurations.

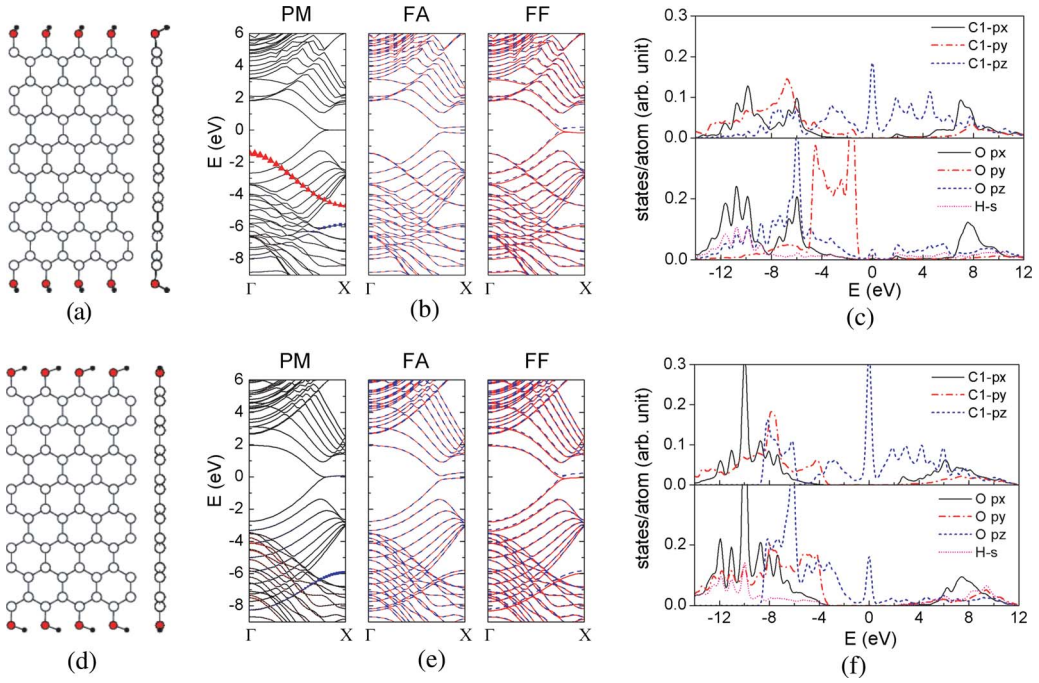

FIG. 7. (Color online) COH-COH: the COH type at both edges. At the first column showing the top and side views of ZGNRs, (a) and (d) correspond to COH-α and COH-β edge types, respectively. The red and black circles mean O and H atoms, respectively. At the second column, (b) and (e), the band structures are shown for three spin configurations. In the PM case, the red triangle (blue rectangle) represents the O-p_y (O-p_z) contribution proportional to the symbol size. At the third column, (c) and (f), the projected DOSs are given for the PM spin configuration.

C. Edge oxidation

The ZGNR band structures are presented for three types of edge oxidation which include hydroxyl (COH-COH), ketone (CO-CO), and ether (C2O-C2O) groups at both edges. By comparing the results with the edge-hydrogenized ZGNRs, we could see that the COH is similar to CH, while the CO and C2O are similar to CH2. In contrast to hydrogenated ZGNR, however, the CO or C2O-oxidized ZGNR always gives metallic band structures because of a correlation between O-p_z and C-π orbitals and larger electronegativity of oxygen than carbon.

1. Hydroxyl (COH-COH)

Hod *et al.*[25] have shown that hydroxyl bonding at ZGNR edges is much more stable than other oxidation groups. This indicates that COH is the most probable structure for the ZGNR edge chemistry. There are two possible COH structures at the edge. Their structures are shown in Figs. 7(a) and 7(d). In Fig. 7(a) COH is bent along the ribbon normal direction, and in Fig. 7(d) it is bent along the ribbon axis direction. Our calculation shows that the latter case has 1.75 eV/u.c. lower energy than the former due to the hydrogen bonding between two OH groups. Such hydrogen bonding, however, is hardly observed, because homogeneous OH bonding along the edge is less likely to occur. If a different chemical group appears in proximity to OH, COH would be bent along the normal direction as in Fig. 7(a), which is more realistic. We note that both of two theoretical studies on the electronic structure of the COH-passivated ZGNR have reported a zero gap only for Fig. 7(a) form.[25,26]

We find that the π-band structures of Figs. 7(a) and 7(d) are very similar and independent of the COH bending direction. In Figs. 7(b) and 7(e), we give the band structures for Figs. 7(a) and 7(d), respectively. Since an oxygen atom has two singly occupied p orbitals, it forms two σ bonds with the H-s and the edge C1-p_x orbitals. So, the OH group makes the edge C1 atom hybridized in a sp^2 form. As one can see from Figs. 7(b) and 7(e), the resulting band structures are very close to that of the CH-CH ZGNR, including the effect of spin polarization. The calculated energy gap is 0.25 (0.13) eV for Fig. 7(b)-FA [Fig. 7(e)-FA], and the other cases are metallic. The FF and FA of Fig. 7(a) [Fig. 7(d)] have 40 (18) and 41 (19) meV/u.c. lower energies than the PM, respectively. Also, the magnetic moments are 0.45 for the FF, and zero for the other cases.

Unlike the CH-CH case, COH-COH ZGNR shows two new bands caused by the O atoms, which are indicated by the red triangles and the blue rectangles in the PM band structures of Figs. 7(b) and 7(e). In order to characterize these bands, we show the corresponding pDOS in Figs. 7(c) and 7(f). From Fig. 7(c), the O-p_z shows a high peak at -6 eV in hybridization with the H-s at lower energy, and the main peak gives one additional π band [indicated by the blue rectangles in Fig. 7(b)] below the bulk C-π bands. The O-p_x forms σ bond with C1-p_x, and the O-p_y behaves like a lone pair whose band is indicated by the red triangles at $-5 < E < -2$ eV in Fig. 7(b). In Fig. 7(f), the O-p_z hybridizes with the C1-p_z orbital, but its π band appears at a significantly lower energy than the bulk C-π bands as indicated by the blue rectangles in Fig. 7(e). The O-p_y and O-p_x orbitals form σ bonds with H-s and C1-p_x, respectively. One can see, in

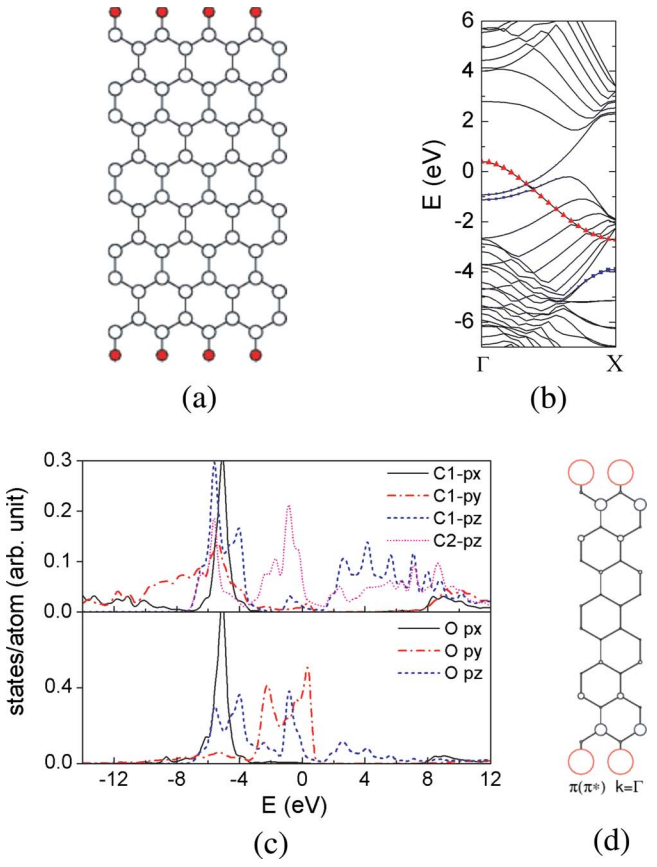

FIG. 8. (Color online) CO-CO: the CO type at both edges. (a) Top view of the ZGNR. (b) The band structure. The PM, FA, and FF spin configurations yield the same band structure shown above. The red triangle (blue rectangle) represents the O-p_y (O-p_z) contribution proportional to the symbol size. (c) The projected DOS for the edge (C1), the inner edge (C2) carbon, and the oxygen (o) atoms. (d) The spatial map of π-orbital contributions for the π-top and π^*-bottom states at $k=\Gamma$ in (b). The red circle means the O-p_z orbital.

Fig. 7(e), the π band caused by O-p_z is pronounced (note that the symbol size is proportional to the contribution of the specific orbital).

2. Ketone (CO-CO)

Figure 8(a) shows the top view of ZGNR with the CO-CO edge type. Its band structure is shown in Fig. 8(b), where all three spin configurations yield the same band structure. The two singly occupied $2p$ orbitals of the O atom are expected to form one σ and one π bond with the edge C atom (C1). Accordingly, the C1-π orbitals will be passivated. So the overall shape of the band structure shown in Fig. 8(b) is similar to that of the CH2-CH2 ZGNR. However, the edge states ($0 \leq k \leq 2\pi/3$) of Fig. 5(b) move below the Fermi level in Fig. 8(b), which yields a metallic band structure. The zero gap in our result is consistent with that of two theoretical reports.[25,26] Our result also shows that there are two bands crossing the Fermi level, one of them being the π^*-bottom band and the other being the O-p_y lone-pair band (indicated by the red triangles).

We show the pDOS in Fig. 8(c) to illustrate the metallic band structure. In the $-6 < E < -4$ eV range, the C1-p_x and O-p_x show a strong hybridization to form a σ bond between them. One can also see that the C1-p_z is mostly passivated to form a π bond with O-p_z near the same energy range. Instead, the C2-p_z has a large peak near the Fermi level, which is why the band structure is similar to the CH2-CH2 case. Above -4 eV, O-p_y peaks appear, and they give rise to the O-p_y lone-pair band in Fig. 8(b) with some empty states at its top. One important feature is that the O-p_z orbital is significantly correlated with the inner edge C2-p_z orbital just below the Fermi level. Since the single electron occupied in the O-p_z orbital has already formed the π bond with the C1, it needs additional electrons to fill the O-p_z peak near the top of valence band. The additional electrons for this resonance are provided by the O-p_y lone-pair band. Thus, the O-p_y band is not fully occupied and the π^* bottom is partially occupied, resulting in the metallic band structure.

The significant correlation between O-p_z and C2-p_z results from the fact that the O atom sits on the same sublattice of the C2 atom. This resonance feature is illustrated in Fig. 8(d) for the π-top and π^*-bottom states at $k=\Gamma$, where the O-p_z orbital behaves like an edge π orbital.

3. Ether (C2O-C2O)

Figure 9(a) shows the top view of a ZGNR with the C2O-C2O edge type. Its band structure is shown in Fig. 9(b), and is the same for all the three spin configurations. We see that the π electronic band structure is similar to that of the CH2-CH2 ZGNR from Figs. 9(b) and 5(a). Although the overall shape is similar, the edge states ($0 \leq k \leq 2\pi/3$) at the Fermi level have significant dispersion in Fig. 9(b), causing a metallic band. Such states are slightly above the Fermi level, and they are less occupied than the CH2-CH2 case.

In order to understand the metallic band structure, we consider the pDOS in Fig. 9(c). The O-p_y forms a σ bond with the inner edge C2-p_y near -12 eV, and the corresponding σ^* states appear at 6 eV. The O-p_x behaves like a lone pair, appearing near -7 eV. Its states are indicated by the black circles in Fig. 9(b). The O-p_z orbital hybridizes with the inner edge C2-p_z, and it creates a new π band at low level, $-10 < E < -6$ eV, as indicated by the blue rectangles in Fig. 9(b). Two p_z electrons are needed to fill this low-lying π band, one from C2-p_z and the other from O-p_z, but C2 has only $\frac{2}{3}$ p_z electron allowed for the π bonding with the O atom. The amount of $\frac{1}{3}$ p_z electron is provided from the filled edge states near the Fermi level, which makes those states less occupied than the CH2-CH2 case. A significant hybridization between C2-p_z and O-p_z also appears near the Fermi level. This causes the dispersion of the edge states along the ribbon axis. Because of the O-p_z, the C2O-C2O ZGNR shows a metallic band structure.

D. Combination of hydrogenation and oxidation

We now consider oxidation at one edge and hydrogenation at the other edge. We need to mention that the different chemical groups within the same edge are more realistic than one type, and it could be an important factor to get semicon-

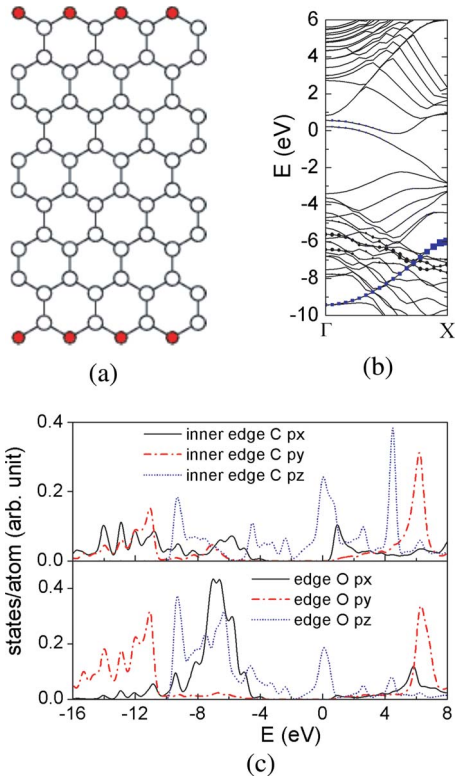

FIG. 9. (Color online) C2O-C2O: the C2O type at both edges. (a) Top view of the ZGNR. (b) The band structure. The PM, FA, and FF spin configurations yield the same band structure shown above. The black circle (blue rectangle) represents the O-p_x (O-p_z) contribution proportional to the symbol size. (c) The projected DOS for the inner edge (C2) carbon and the oxygen (O) atoms.

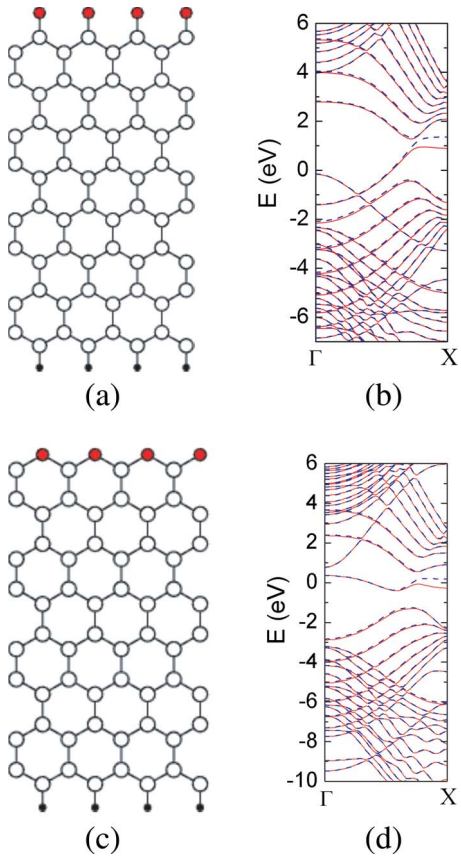

FIG. 10. (Color online) (a) ZGNR for the CH-CO edge type, and (b) its band structure for the FA spin configurations. (c) ZGNR for the CH-C2O edge type, and (d) its band structure for the FA spin configurations. For both types of ZGNR, the FF spin configuration gives the same band structure as the FA.

ducting character of GNRs as will be discussed later. However, such task demanding a larger supercell and more computational time is beyond the scope of our current study, and we focus on homogenous edge structure in this paper. We have shown that OH passivation yields almost the same π-band structure as the H passivation. So, we do not consider OH passivation, but consider the CH or CH2 type at one edge, and the CO or C2O at the other edge. When two edges are passivated by different functional groups, the chemical potential difference in edge groups will induce a charge transfer from one edge to the other leading to a potential difference (ΔV) between the edges and the corresponding internal electric field ($E=\Delta V/W$). In our periodic supercell calculations, the potential difference between the edges is accommodated by introducing an electric dipole plane in the middle of periodic images (see Ref. 34).[33]

Figure 10 shows the ZGNR structures and their band structures for one edge passivated with CH. Since CO or C2O induces sp^3 hybridization of the edge C atoms, we expect to see a flat band near the Fermi level, as in the CH-CH2 case. It can be seen that the band structure has nearly the same shape as that of CO (C2O) for $0 \leq k \leq 2\pi/3$, and that of CH for $2\pi/3 \leq k \leq \pi$. For $2\pi/3 \leq k \leq \pi$, there are H-related edge states, and they follow the same trend as that of CH-CH for the FA or FF variation of spin configuration (only the FA result shown in Fig. 10). For $0 \leq k \leq 2\pi/3$, the CO or C2O edge yields the metallic band caused by the C-O chemical interaction. Due to the chemical potential difference between the C-O and CH edges, the CO (CH) related states shift down (up) compared to the CO-CO (CH-CH) case as shown in Fig. 10(b). Consequently, the O-p_y lone-pair band is fully occupied and the CH-related flat bands are empty. However, similar edge state shifts do not happen in case of CH-C2O since oxygen is fully saturated and no charge transfer is allowed. As shown in Fig. 10(d), the dispersive π band crosses the Fermi level for CH-C2O band structure.

Figure 11 shows the top views and band structures of the ZGNR with one edge passivated in the CH2 form. Since both edges have a chemical environment similar to that of sp^3 hybridization, the resulting band structures are expected to be similar to that of the CH2-CH2 case. The band structures shown in Figs. 11(b) and 11(d) confirm this expectation. The band structures for the three kinds of spin configuration are all the same, and the PM result is shown. Similar to Fig. 10(b), O-p_y band is fully occupied for the CO type, resulting in a band gap. For the C2O type, the result is similar to the C2O-C2O case, but the flat π and π^* bands are less dispersive. As a result, there is a band gap as well.

From Figs. 10 and 11, one can identify an intrinsic π-band structure caused by specific edge chemistry. The variation of edge chemistry at one edge does not change

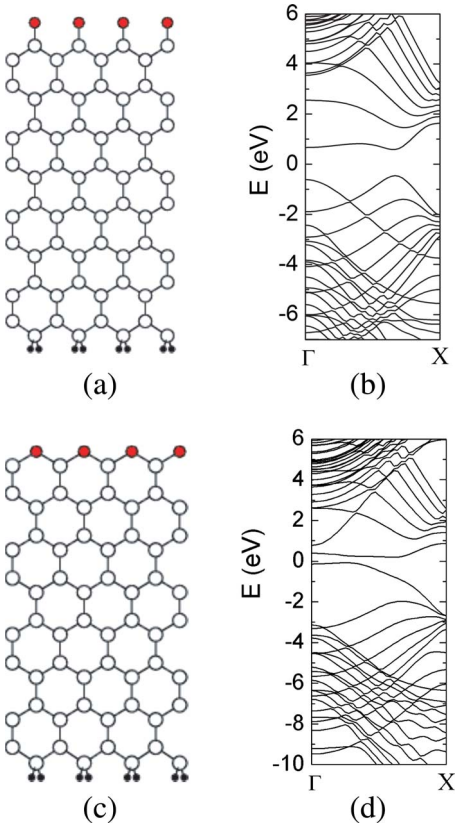

FIG. 11. (Color online) (a) ZGNR for the CH2-CO edge type, and (b) its band structure. (c) ZGNR for the CH2-C2O edge type, and (d) its band structure. The band structures for both types correspond to the PM spin configuration, and they are all the same as the FA and FF spin configurations.

significantly the π-band structure shape of the other edge. This means that the π-band structure near the Fermi level is primarily determined by C-O or C-H chemical interaction at the edge. However, it is worthwhile to note that the chemical potential difference between the edge states has induced a charge transfer between them leading to a potential difference (ΔV) and the corresponding internal electric field ($E=\Delta V/W$). The potential difference is 3 eV corresponding to 0.2 eV/Å internal electric field induced by heterogeneous edge passivation for 8-ZGNR. The potential difference remains as 3 eV for wider GNRs with similar band structures (Ref. 34). Son *et al.*[17] have shown that an externally applied electric field across CH-CH-passivated GNR can close the band gap of FA band structure shown Fig. 4(a), and the required field strength for 8-ZGNR is 0.2 eV/Å corresponding to 3 eV potential difference between the edges. This comparison provides an insight on the underlying mechanism for metallic band structure formation for oxide-passivated GNRs as the metallic bands in Figs. 8 and 9 are driven by the electron loss of π bands to oxygen orbitals leading to partially occupied π bands.

IV. DISCUSSION

Our calculated ZGNR band structures for H or H2 passivation for sp^2 or sp^3 hybridization of edge C atoms are consistent with other theoretical results.[15–17,23,24] For oxidation of edge C atoms, we have seen that the COH-COH ZGNR gives nearly the same π-band structure as the CH-CH ZGNR, and that the π-band structure of CO-CO or C2O-C2O ZGNR is similar to that of the CH2-CH2 ZGNR. Such similarities come from the fact that the π-band structure of ZGNR is determined by whether the edge C atom is hybridized in a sp^2 or sp^3 form (i.e., the hybridization type of C1). Furthermore, the π orbital states near the Fermi level have similar localization characteristics under the same hybridization type of C1. This analysis is represented in Fig. 12 which shows the one-dimensional profile of the π-orbital contribution along the transverse direction for the six types of edge chemical modification of 8-ZGNR. We have chosen the states within +1 and −1 eV from the Fermi level for each band structure, and computed the average value with the number of states within that range. Profiles belonging to the same hybridization type of C1 are shown in the same panel. For CH-CH and COH-COH, the magnitude decreases exponentially away from the edge. Near the edge, the magnitude at the different sublattice from one of edge C is always close to zero, but the magnitudes at both sublattices become similar at the center. For CH2-CH and CH2-CH2, it is nonzero at the inner edge site for the CH2 side. For CO-CO, the magnitudes are almost the same at all of the same sublattice sites, which indicates that the edge states are delocalized over the whole ribbon. Such delocalization was also reported for the ketonated graphene nanodot.[27] For C2O-C2O, the magnitudes exponentially decay, but at one of the two sublattices they are not close to zero.

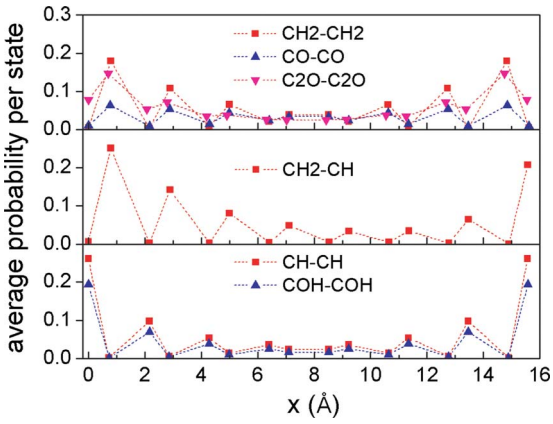

FIG. 12. (Color online) The π-orbital contribution profile of every C atom along the transverse direction of the ZGNR with six kinds of edge-chemistry modifications. All the ZGNRs have the width of 8 zigzag chains and their structures are shown in Figs. 4–9. The magnitude is averaged over the states within +1 and −1 eV from the Fermi level. The x axis denotes the transverse distance (in Å) relative to one edge C atom.

Although the overall band structures are similar between edge-hydrogenated and oxidized ZGNRs, the oxidation gives different features from the hydrogenation. First, the O-p_z produces one additional π band which is similar to C-π bands for COH, CO, and C2O types. Its energy level is lower than C-π bands because oxygen p orbital energy is lower than that of carbon. Second, the band structures are metallic

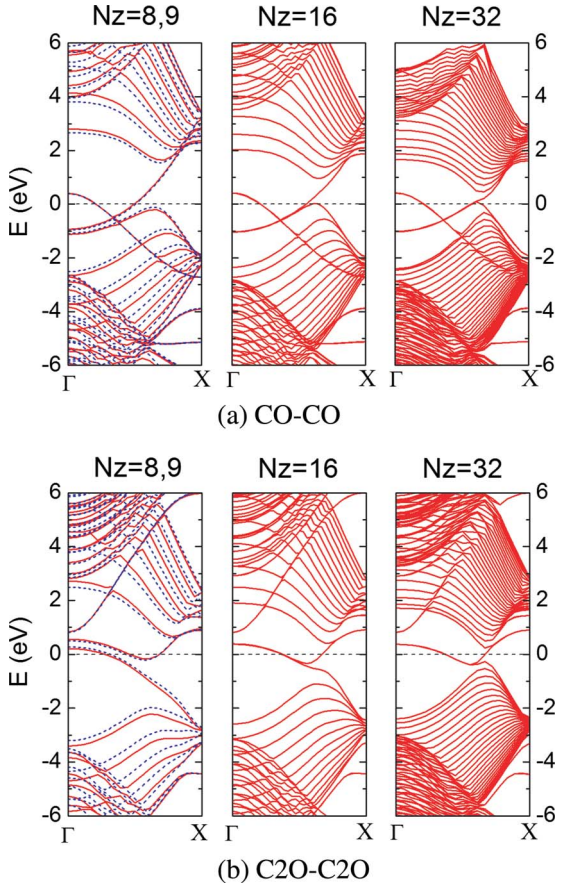

FIG. 13. (Color online) Band structures of (a) CO-CO and (b) C2O-C2O ZGNRs with the widths of 8, 16, and 32 zigzag chains which correspond to 1.6, 3.2, and 6.4-nm width, respectively. Also the results of 9 zigzag chains are shown with the blue dashed line in the Nz=8,9 to show their similar band structures except to the number of subbands.

for CO and C2O types. For the CO type, the O-p_z appearing at the same sublattice of C2 atom is significantly hybridized with C2-π orbitals by which the edge states are mostly formed. Since the high electronegativity of oxygen tends to stabilize the edge states, they are shifted a little below the Fermi level. This shift makes the π^*-bottom band to be partially filled since additional electrons are donated from O-p_y. For the C2O type, the lack of electrons in forming a stable π bond between O and C2 atoms is compensated from C2-p_z electrons. As a result, the edge states are shifted above the Fermi level making π-top band slightly empty.

The metallic band structures for the CO-CO and C2O-C2O ZGNRs are primarily caused by the difference in electronegativity between C and O atoms. Since the interaction between C and O is localized at the edges, widening edge-oxidized ribbons cannot eliminate such metallic band structure. To confirm this prediction, the band structure of CO-CO and C2O-C2O ZGNRs with larger ribbon widths are calculated and shown in Fig. 13. The left panel of Fig. 13(a) shows the CO-CO ZGNR for N_Z=8 and 9, and the main difference is the increased number of π and π^* bands for 9-ZGNR with practically identical band structure near the Fermi level. As the ZGNR width further increases to 16 and 32, the number of π and π^* bands correspondingly increase, and the highest π and the lowest π^* bands become degenerate for $k<2\pi/3$. The two metallic bands crossing the Fermi level remain the same while N_Z is changing. Figure 13(b) shows the same properties of C2O-C2O ZGNRs as N_Z is increasing from 8 to 9, 16, and 32.

Our calculated band structures of ZGNRs with edge hydrogenation and oxidation are not consistent with the observed semiconducting behavior of GNRs.[13,14] For the CH, CH2, and COH types, we have seen an energy gap only in the case of a particular spin configuration, and the energy difference between different spin configurations is very small (on the order of 1 meV/atom). For experimental measurements at room temperature, it is not likely that one specific spin configuration would be strongly favored. For the CO and C2O types, the metallic band structures were obtained in contrast to an ordinary fact that materials transform into insulators upon oxidation. The dispersive character of the metallic bands indicates that the edge-oxidized ZGNRs will show metallic transport behavior in contrast to the measurement data. The GNRs used in experimental studies are prepared by oxygen plasma etching[13] or intercalation of oxidizing acids[14] so that the GNR edges will be oxidized rather than hydrogen passivated.

The discrepancy on GNR band gap opening between our results and the experiments requires further analysis on the effects of GNR edge structures. In this paper, we have examined uniform chemical modification of straight GNR edges for both hydrogenation and oxidation. In order to develop realistic GNR model structures with edge-related electrical properties comparable to experimental data, one should extend the current modeling study by including edge roughness and chemical disorder. Since it is shown that the edge roughness does not reduce the conductance of ZGNRs,[20–22] the chemical disorder would be the most likely reason for the semiconducting behavior shown in experimental GNR samples. It has been shown that low O coverage at ZGNR edges instigates the metal-semiconductor transition,[26] where energy gaps of 0.82 and 0.41 eV were obtained for the up and down spin states, respectively. Another important effect is the chemical adsorption of atoms or molecules onto the basal plane of GNRs. For example, the epoxides and hydroxyls on the graphene basal plane are known to form insulating graphene oxides[35] even though the atomic structures are not fully understood yet. During the GNR sample preparations using oxygen plasma etching,[13] O atoms can easily diffuse on the graphene basal plane near the edges leading to the inactive edge width W^* observed in the GNR transport measurements. Similarly, the graphene basal planes would be modified by intercalation of oxidizing acids during the preparation of ultrasmooth GNRs consistent with the low mobility values of 100–200 cm^2/Vs.[14] There are additional factors contributing to the experimentally measured transport behavior of GNRs such as substrate effect and metal-graphene contact effect. Large scale impurities or potential variation of the substrate may induce charge inhomogeneity leading to interpenetrating electron and hole puddles.[11] A strong localization of such puddles can introduce a transport gap in the conductance measurement. Finally, graphene-metal contact could block the injection of carriers from elec-

trodes depending on the bonding character at the interface. These are the topics of our current graphene modeling research and we will report the findings elsewhere.

V. SUMMARY

We have calculated the band structures of edge-chemistry-modified ZGNRs using the *ab initio* density-functional method with LSDA. Our results for ZGNRs with CH, CH2 (H passivations), COH, CO, and C2O (oxidations) show that the bare ZGNR is more likely to be oxidized than hydrogenated. We have confirmed that our results are consistent with other theoretical results for the H passivations, and we have compared the band structures of the edge-oxidized ZGNRs with those of hydrogenated ZGNRs. We found that an oxidation by the OH group gives almost the same band structure as a single H passivation (sp^2 hybridization) does, and that the ketone (CO) and ether (C2O) groups are similar to H2 passivation (sp^3 hybridization). Our results show that ZGNRs with CO or C2O edge modification always become metallic. The origin of their metallic band structures is the chemical interaction between edge C and O atoms, mainly caused by the difference in electronegativity. For the ketone group, there is a partial electron transfer from the oxygen lone pair (O-p_y) to the O-p_z orbital to fill the π^*-bottom band. For the ether group, the π-top band donates some electron charge into the O-p_z to saturate the stable π bond between O and nearby C atoms, and becomes partially occupied. Our study indicates that we need to consider more realistic GNR model structures including chemical disorder and impurities at the ribbon edge in order to clarify the origin of the semiconductor behavior in experimental GNR samples.

ACKNOWLEDGMENTS

This work was supported by the EMMITT fund through UTD and the NRI SWAN Project. We thank graphene research group members in UTD for helpful discussions.

*kjcho@utdallas.edu

[1] A. K. Geim and K. S. Novoselov, Nature Mater. **6**, 183 (2007).
[2] K. S. Novoselov, A. K. Geim, S. V. Morozov, D. Jiang, Y. Zhang, S. V. Dubonos, I. V. Grigorieva, and A. A. Firsov, Science **306**, 666 (2004).
[3] Y. Zhang, Y.-W. Tan, H. L. Stormer, and P. Kim, Nature (London) **438**, 201 (2005).
[4] C. Berger *et al.*, Science **312**, 1191 (2006).
[5] F. Schedin, A. K. Geim, S. V. Morozov, E. W. Hill, P. Blake, M. I. Katsnelson, and K. S. Novoselov, Nature Mater. **6**, 652 (2007).
[6] M. C. Lemme, T. J. Echtermeyer, M. Baus, and H. Kurz, IEEE Electron Device Lett. **28**, 282 (2007).
[7] Z. Chen, Y. Lin, M. J. Rooks, and Ph. Avouris, Physica E (Amsterdam) **40**, 228 (2007)
[8] X. Wang, Y. Ouyang, X. Li, H. Wang, J. Guo, and H. Dai, Phys. Rev. Lett. **100**, 206803 (2008).
[9] J. Kong, N. R. Franklin, C. Zhou, M. G. Chapline, S. Peng, K. Cho, and H. Dai, Science **287**, 622 (2000).
[10] Yu-Ming Lin, J. Appenzeller, Z. Chen, Z.-G. Chen, H.-M. Cheung, and Ph. Avouris, IEEE Electron Device Lett. **26**, 823 (2005).
[11] J. Martin, N. Akerman, G. Ulbricht, T. Lohmann, J. H. Smet, K. von Klitzing, and A. Yacoby, Nat. Phys. **4**, 144 (2008).
[12] Y.-W. Tan, Y. Zhang, K. Bolotin, Y. Zhao, S. Adam, E. H. Hwang, S. Das Sarma, H. L. Stormer, and P. Kim, Phys. Rev. Lett. **99**, 246803 (2007).
[13] M. Y. Han, B. Ozyilmaz, Y. Zhang, and P. Kim, Phys. Rev. Lett. **98**, 206805 (2007).
[14] X. Li, X. Wang, L. Zhang, S. Lee, and H. Dai, Science **319**, 1229 (2008).
[15] K. Nakada, M. Fujita, G. Dresselhaus, and M. S. Dresselhaus, Phys. Rev. B **54**, 17954 (1996).
[16] Y. Miyamoto, K. Nakada, and M. Fujita, Phys. Rev. B **59**, 9858 (1999).
[17] Y.-W. Son, M. L. Cohen, and S. G. Louie, Phys. Rev. Lett. **97**, 216803 (2006); Nature (London) **444**, 347 (2006).
[18] V. Barone, O. Hod, and G. E. Scuseria, Nano Lett. **6**, 2748 (2006).
[19] L. Yang, C.-H. Park, Y.-W. Son, M. L. Cohen, and S. G. Louie, Phys. Rev. Lett. **99**, 186801 (2007).
[20] D. A. Areshkin, D. Gunlycke, and C. T. White, Nano Lett. **7**, 204 (2007).
[21] F. Munoz-Rojas, D. Jacob, J. Fernandez-Rossier, and J. J. Palacios, Phys. Rev. B **74**, 195417 (2006).
[22] T. C. Li and S.-P. Lu, Phys. Rev. B **77**, 085408 (2008).
[23] K. Kusakabe and M. Maruyama, Phys. Rev. B **67**, 092406 (2003).
[24] H. Lee, Y.-W. Son, N. Park, S. Han, and J. Yu, Phys. Rev. B **72**, 174431 (2005).
[25] O. Hod, V. Barone, J. E. Peralta, and G. E. Scuseria, Nano Lett. **7**, 2295 (2007).
[26] F. Cervantes-Sodi, G. Csanyi, S. Piscanec, and A. C. Ferrari, Phys. Rev. B **77**, 165427 (2008).
[27] H. Zheng and W. Duley, Phys. Rev. B **78**, 045421 (2008).
[28] P. W. Anderson, Phys. Rev. Lett. **34**, 953 (1975).
[29] G. Kresse and J. Hafner, Phys. Rev. B **47**, 558 (1993); G. Kresse and J. Fürthmuller, *ibid.* **54**, 11169 (1996).
[30] P. E. Blöchl, Phys. Rev. B **50**, 17953 (1994); G. Kresse and D. Joubert, *ibid.* **59**, 1758 (1999).
[31] D. M. Ceperley and B. J. Alder, Phys. Rev. Lett. **45**, 566 (1980).
[32] The use of Gaussian broadening with the width 0.25 eV gives metallic feature in pDOS.
[33] J. Neugebauer and M. Scheffler, Phys. Rev. B **46**, 16067 (1992).
[34] See EPAPS Document No. E-PRBMDO-79-078916 for electrostatic potential profiles with and without dipole correction, and for its dependence on the GNR width. For more information on EPAPS, see http://www.aip.org/pubservs/epaps.html.
[35] S. Stankovich, D. A. Dikin, G. H. B. Dommett, K. M. Kohlhaas, E. J. Zimney, E. A. Stach, R. D. Piner, S. T. Nguyen, and R. S. Ruoff, Nature (London) **442**, 282 (2006).